

Infrared absorption in bismuth nanowires resulting from quantum confinement

M. R. Black,^{1,*} Y.-M. Lin,¹ S. B. Cronin,² O. Rabin,³ and M. S. Dresselhaus^{1,2}

¹*Department of Electrical Engineering and Computer Science, Massachusetts Institute of Technology, Cambridge, Massachusetts 02139-4307*

²*Department of Physics, Massachusetts Institute of Technology, Cambridge, Massachusetts 02139-4307*

³*Department of Chemistry, Massachusetts Institute of Technology, Cambridge, Massachusetts 02139-4307*

(Received 8 October 2001; revised manuscript received 26 February 2002; published 2 May 2002)

Results are reported for experimentally measured and theoretically predicted optical absorption in bismuth nanowires. Five absorption peaks are seen in the experimental spectral range. The energies of these five peaks agree well with the predicted values for intersubband transitions, thereby validating our model of quantum confinement in bismuth nanowires. We also compare the measured absorption in free-standing wires to the absorption of wires inside an alumina template obtained from an analysis of transmission and reflection measurements using a reverse effective-medium theory. Close agreement between the energies of the largest absorption peak is found by the two methods. The weaker absorption peaks were not observed in the spectrum of wires embedded in alumina.

DOI: 10.1103/PhysRevB.65.195417

PACS number(s): 78.67.Lt, 81.07.Vb

I. INTRODUCTION AND METHODOLOGY

Because of the special band structure of bismuth, bismuth nanowires are an especially interesting system for studying quantum confinement. Bismuth is a semimetal with a small band overlap (38 meV at 0 K) and a very anisotropic electron effective mass tensor (varying from $0.001m_0$ to $0.26m_0$, depending on the crystalline direction).¹ For a Bi nanowire of small enough diameter for significant quantum confinement to occur, the nanowire undergoes a transition from a semimetal with a small band overlap to a semiconductor with a small direct band gap. This transition, as well as other quantum effects, occur in Bi nanowires at relatively large wire diameters because of the small effective mass and small band overlap of bulk bismuth. For example, in nanowires oriented along the (012) crystalline direction (such as our wires²), this transition is predicted to occur at a diameter of 49 nm at 77 K.³

In addition to the thermoelectric applications previously proposed for Bi nanowires,⁴ Bi nanowires also hold promise for optical applications because of their unusual properties. For example, quantum wells, quantum dots, and quantum wires usually have to be doped in order to populate the lowest subband and to allow for optical excitation of the electrons to higher subbands. However, since the direct band gaps for our wires are smaller than $3k_B T$ at room temperature, the lower subbands are partially filled with electrons even in undoped samples, and intersubband transitions can be observed. In addition, one-dimensional systems exhibit singularities in the joint density of states, allowing subbands in Bi nanowires to be readily observable even at room temperature. More importantly, the selection rules for intersubband transitions in arrays of quantum wires, such as our bismuth nanowires, allow optical absorption to occur for light incident perpendicular to the sample (in-plane absorption). In-plane optical absorption greatly simplifies device testing, improves the ease of measurements, and may make Bi nanowires useful for optical applications. For all of these reasons and many others, Bi nanowires provide an interest-

ing system for studying quantum confinement and in particular intersubband transitions.

The Bi nanowires used in this study are fabricated utilizing the pores of an anodic alumina template,^{5,6} which serves as a host material. Since alumina is a wide-band-gap semiconductor, individual wires which are fixed in place are electrically isolated from each other. The direct (L -point) interband transition energy increases with decreasing nanowire diameter, and for Bi nanowires, quantum confinement effects are significant for diameters less than about 50 nm. At room temperature, for example, the direct bandgap of bulk bismuth (the L point) is 36 meV (290 cm^{-1}), while for 40-nm wires, we calculate the direct band gap to be 123 meV (990 cm^{-1}). In the frequency range of our experiments, the wavelength of light is more than 50 times greater than the wire diameter. As a result, both the alumina host material and the Bi nanowires contribute to the measured optical properties. The contribution of the nanowires can be separated from that of the measured nanowire/dielectric composite by making use of an effective-medium theory (EMT) formalism.⁷⁻¹⁰ Here we use an EMT in reverse to obtain the dielectric function of the Bi nanowires inside the alumina when the dielectric function of the composite material is known.¹¹

In this paper we present both experimental measurements and results of model calculations of the optical absorption from quantum confinement in bismuth nanowires. Section II explains how effective medium theory is used in reverse to deconvolve the dielectric function of bismuth nanowires embedded in alumina. In Sec III, the results from this method are compared to absorption measurements of free-standing bismuth nanowires. In Sec. IV of the paper, we present a theoretical model to simulate the absorption from both interband and intersubband transitions in bismuth nanowires as a function of the wave number. The results of this model are then compared to the results of the absorption observed in the free-standing wires. Conclusions are given in Sec. V.

II. REVERSE EFFECTIVE-MEDIUM THEORY

Unfortunately since the wire diameter is much smaller than the wavelength of light used in this study, the absorption

of the alumina cannot simply be subtracted out from the absorption of the bismuth-alumina composite. Obtaining the dielectric function at wavelengths much longer than the feature size of the sample requires extracting the relevant information from measurements on a composite sample, which in our case includes bismuth nanowires embedded in an alumina template.

Many prior studies have developed an effective-medium theory for predicting the dielectric function of a composite material when the dielectric function of both the constituent materials are known.^{9,12–14} When a sample is composed of more than one material, with the size of the constituents smaller than the wavelength (λ) of the optical fields, an effective-medium theory treats this inhomogeneous material as a single material with a single dielectric function. In the present study we utilize the Maxwell-Garnett (MG) EMT,^{13,14} which is valid for nanoparticles smaller than λ inside a dielectric material. We choose the MG EMT, since it agrees with an exact calculation done for the case of cylindrical pores in alumina.¹⁰ The MG EMT relates the dielectric function of the composite material to that of the guest (bismuth or air) and host (alumina) material by

$$\frac{\epsilon_{\text{composite}} - \epsilon_{\text{host}}}{\epsilon_{\text{composite}} + K * \epsilon_{\text{host}}} = f \frac{\epsilon_{\text{guest}} - \epsilon_{\text{host}}}{\epsilon_{\text{guest}} + K * \epsilon_{\text{host}}}, \quad (1)$$

where K is the screening parameter and f is the volume fraction of the guest material in the composite material. For infinitesimally small nanowires, $K=1$ and the solution equals that given in Ref. 10. Several research groups have used EMT to identify the dielectric function of a composite materials, $\epsilon_{\text{composite}}$, using ϵ_{host} and ϵ_{guest} of the constituents.^{7,8,15–22} In this study, we use a reverse EMT to deduce the dielectric function of the guest material when the dielectric functions of the composite and of the host material are found by experimental measurements.

The dielectric function of the bismuth/alumina composites and the air/alumina composites are found by one of two methods described below. One method uses Kramers-Kronig relations to obtain the dielectric function of the composite material from the measured reflection as a function of wave-number. The second method uses the solution of Maxwell's equations for a thin slab to simulate the reflection and transmission. For each data point, by adjusting the complex dielectric constant of the thin slab, the mean-square error between the measured and calculated reflection and transmission values is minimized. The Kramers-Kronig method is accurate when the transmission is small, while the Maxwell method is accurate when both the transmission and the reflection are both large enough to be measured. For most of our samples, the transmission is small but measurable, so either method can be used, although neither method is perfect. In the present study the two methods were compared and found to yield similar results for the real and imaginary components of the dielectric function for bismuth-filled alumina templates.

Once the dielectric function of the bismuth/alumina composite is obtained, EMT is used in reverse to find the

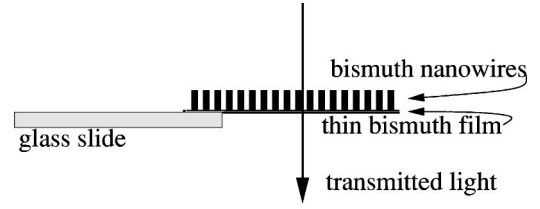


FIG. 1. A schematic diagram of a free-standing bismuth nanowire array mounted on a glass slide.

dielectric function of the bismuth nanowires. From Eq. (1), the dielectric function of the nanowires is described by the equation

$$\epsilon_{\text{guest}} = \epsilon_{\text{host}} \frac{K \epsilon_{\text{composite}} - K \epsilon_{\text{host}} + f \epsilon_{\text{composite}} + f K \epsilon_{\text{host}}}{-\epsilon_{\text{composite}} + \epsilon_{\text{host}} + f K \epsilon_{\text{host}} + f \epsilon_{\text{composite}}}, \quad (2)$$

and this reverse EMT was used in Ref. 11 to obtain the dielectric function of bismuth nanowires as a function of diameter.

III. EXPERIMENTAL RESULTS

Porous anodic aluminum oxide templates are fabricated by anodizing aluminum sheets in an oxalic acid solution.⁵ During this process, cylindrical pores 7–200 nm in diameter are self-assembled into a hexagonal array. The pore diameter and the distance between the pores can be controlled systematically by varying the anodization voltage and the electrolyte used.^{23,24} The thickness of the alumina template determines the wire length, and can be controlled by the anodization time. The thickness of samples used in this study are 40–60 μm . The pores in the alumina templates are filled with Bi using a pressure injection technique.⁵

The optical reflection $R(\omega)$ and transmission $T(\omega)$ were measured as a function of frequency at room temperature using a Nicolet Magna-IR 860 spectrometer and the Nic-Plan IR Microscope. The microscope Fourier transform infrared spectrometer allows transmission and reflection measurements through a microscope stage and therefore enables measurements of 1–2-mm samples. Reflection data were taken in the infrared region from $600 < 1/\lambda < 4000 \text{ cm}^{-1}$ at 293 K using a gold film as a comparison standard. The resolution was 2 cm^{-1} .

In order to test the validity of the reverse EMT method for obtaining the dielectric function of bismuth nanowires, we measured the absorption of free-standing bismuth nanowires without an alumina template. First, the alumina template was etched off using a selective etch leaving only bismuth behind. Using the microscope FTIR, the reflection and transmission were measured from a sample, containing the free-standing Bi nanowires, a bismuth oxide coating over the nanowires, and a thin Bi film holding the nanowires together. A schematic diagram of the sample is shown in Fig. 1. A thin piece of bismuth with nanowires protruding like blades of grass is balanced on the edge of a glass slide, while light is transmitted through the sample in the direction of the wires so that the electric field of the incident light is always perpendicular to the wire axis. Since the transmission is proportional to e^{-Kd} , where K is the absorption coefficient and d is

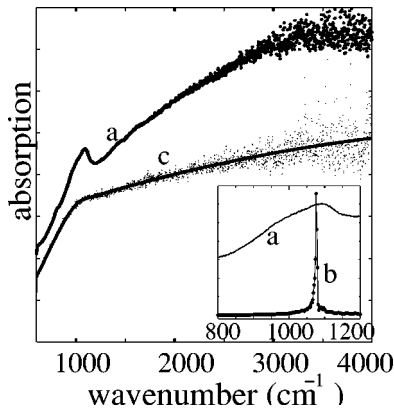


FIG. 2. The frequency dependence of the absorption coefficient found by taking the negative log of the transmission of free-standing bismuth nanowires (a), as well as the absorption on a thin piece of bismuth (points) and the fit to this absorption (line curve) (c). The inset compares the absorption of the free-standing wires (a), with the absorption coefficient $[\text{Im}(\epsilon_1 + i\epsilon_2)]^{1/2}$ of bismuth nanowires inside an alumina template (b) as obtained by reverse EMT. The main absorption peaks of the two samples occur at about the same photon energy.

the sample thickness, the negative log of the transmission is proportional to the absorption coefficient. Since the thickness of the template is poorly determined, the absolute magnitude of the absorption coefficient cannot be obtained quantitatively. The absorption coefficient (times the sample thickness), as a function of the wave number, obtained by taking the negative log of the transmission intensity of the free-standing bismuth nanowires, is shown in Fig. 2 (a). For comparison, Fig. 2 also shows the absorption coefficient from ~ 40 -nm Bi nanowires inside an alumina template curve (b), obtained by using the reverse EMT analysis.¹¹ The wires used for the free-standing nanowire measurements had a diameter of 60 nm before the alumina template surrounding the wires was etched away. Since a ~ 7 -nm oxide grows on the free-standing wires after the alumina is selectively etched away,²⁵ the inner bismuth portion of the free-standing wires is expected to have a diameter of around 45 nm. The two

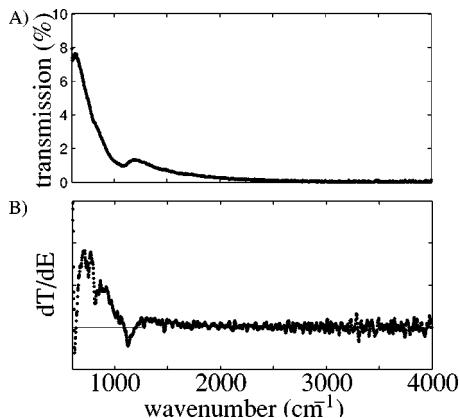


FIG. 3. (A) The transmission as a function of wave number of free-standing bismuth nanowires. (B) The energy derivative of the transmission as a function of wavenumber.

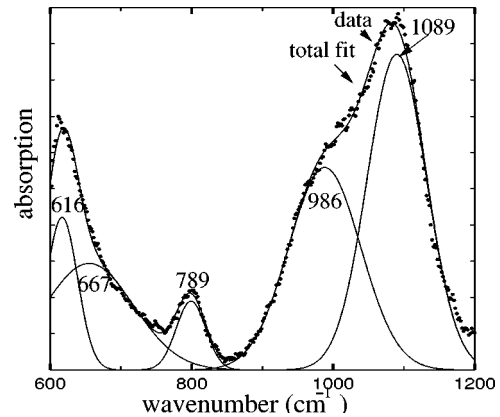


FIG. 4. Fit of Gaussian peaks to the absorption spectrum in the free-standing Bi nanowire sample. Five broad peaks are observed at 616, 667, 798, 986, and 1090 cm^{-1} . The absorption from the thin bismuth sample is used as the baseline, and the absorption due to all five peaks is shown as the “total fit” to the data points.

nanowire arrays are therefore of comparable wire diameters. Figure 2 also includes the absorption of a thin film of bismuth (c), and the curve used to provide the background spectra in fitting the absorption spectra in Fig. 4. Since the thickness of the thin bismuth film holding the bismuth nanowires is not known, the thickness is used as a fitting parameter to find the best background spectra for the measured data. The transmission (A) and the energy derivative of the transmission (B) are shown in Fig. 3. As can be seen from Fig. 3, all the features in the transmission curve are at wavenumbers less than 1500 cm^{-1} . Figure 4 shows the measured absorption of the free-standing wires after the thin bismuth film absorption is subtracted out. Figure 4 also shows a fit of a sum of Gaussian peaks to the absorption in the free-standing nanowires. The absorption of the bismuth oxide is not considered, since bismuth oxide was found to have very little optical absorption in the energy range of our measurements.

The free-standing Bi nanowires absorb strongly at $\sim 1050 \text{ cm}^{-1}$ [curve (a) in Fig. 2], in excellent agreement with the peak absorption energy of Bi wires in the alumina template obtained by the reverse EMT approach [curve (b) in the inset to Fig. 2]. However, the absorption peak is much sharper, absorbing only from 1000 to 1100 cm^{-1} , for the Bi nanowires embedded in the alumina template, than the peak for the free-standing wires which extends from about 950 to 1150 cm^{-1} . The difference in the absorption peak widths may have several explanations. The difference might indicate limitations of the reverse effective-medium theory, since the accuracy of the reverse effective-medium theory depends on the magnitude of the imaginary part of the dielectric function of the host material. By comparing the transmission spectra of the filled and unfilled alumina templates as shown in Fig. 5, we know that the absorption in alumina is large for wave numbers less than 1000 cm^{-1} . We thus expect a decrease in the accuracy of the absorption obtained by reverse effective medium theory for wave numbers less than 1000 cm^{-1} . The difference in absorption peak widths is, however, more likely a result of a widening of the wire diameter *distribution* and inhomogeneity along the length of each wire and among the

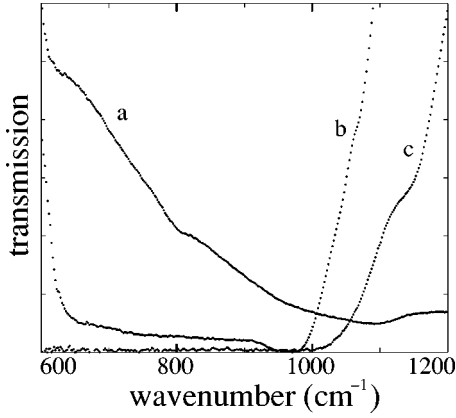


FIG. 5. Transmission data vs wavenumber for (a) free-standing Bi nanowires, (b) an unfilled alumina template, and (c) a Bi-filled alumina template.

various wires during Bi oxide growth after the removal of the alumina template.

In addition to the large absorption peak at $\sim 1050 \text{ cm}^{-1}$, smaller absorption peaks are observed at ~ 616 , ~ 667 , ~ 798 , and $\sim 986 \text{ cm}^{-1}$ in the free-standing Bi nanowires. These peaks were not seen for the nanowires embedded in alumina. This may indicate a decrease in the accuracy or sensitivity of the reverse effective-medium theory in this frequency range, and shows that the reverse EMT method for determining the dielectric function of nanowires smaller than the wavelength of light has limitations that need to be further explored. Even though the experiment, using alumina/Bi nanowire template samples and the reverse EMT, allows us to determine the optical properties of aligned and nonoxidized bismuth nanowires, the alumina template masks the smaller peaks observed in the free-standing wire experiment. We therefore choose to use the data obtained from free-standing wires when comparing experimental and simulated absorption curves.

IV. THEORETICAL MODELING AND NUMERICAL SOLUTIONS

Model calculations are presented in order to understand the intersubband and interband transitions in bismuth nanowires, and hence to gain insight into the mechanism responsible for the absorption peaks observed in the experimental data. Intersubband transitions are suspected to be the cause of the observed optical absorption in bismuth nanowires for several reasons.¹¹ The polarization dependence of the optical absorption is consistent with absorption from intersubband transitions. The absorption is observed when the electric field of the incident light is perpendicular to the wires, but is not observed when the electric field is parallel to the wires. In addition, the energy of the peak absorption was found to increase with decreasing wire diameter, as expected for both interband and intersubband transitions. Also, the energy range where absorption peaks are observed is the energy range in which absorption from intersubband and interband transitions are expected. Finally, the shape and peak width of the measured absorption curve is as predicted for the shape

of the absorption spectrum from intersubband transitions in which the bands track each other.¹¹

A photon can excite an electron to an unfilled higher-energy state if the energy of the photon exactly equals the energy difference between the final and initial states and if momentum is conserved. The photon absorption from this process can be measured by the energy-dependent optical-absorption spectrum. When stimulated emission as well as absorption is accounted for, the optical absorption coefficient for the Bi nanowire quasi-one-dimensional system, as a function of photon energy, $\hbar\omega$, is given by²⁶

$$\alpha_{abs,1D}(\omega) = (\pi e^2 / \epsilon_0 c \eta \omega m^{*2}) \sum_{n,m} (2/2\pi) \times \int dk_z |\langle n|p|m \rangle|^2 [f(E_n) - f(E_m)] \times \delta(E_n - E_m - \hbar\omega), \quad (3)$$

where α is the optical absorption coefficient, ω is the frequency of the incident light, $\langle n|p|m \rangle$ is the momentum matrix element for coupling between the n th and m th states, z is wire axis direction, η is the index of refraction, m^* is the effective mass of the carriers, c is the speed of light, E_n and E_m are the energy of states n and m , respectively, and $f(E_n)$ and $f(E_m)$ are the Fermi-Dirac distribution functions for states n and m , respectively. The imaginary part of the dielectric function, ϵ_2 , can be related to the optical-absorption coefficient by

$$\epsilon_2(\omega) = c \eta \alpha_{abs}(\omega) / \omega. \quad (4)$$

Combining Eqs. (3) and (4), we obtain an expression for the imaginary part of the dielectric function:

$$\epsilon_{2,1D}(\omega) = (\pi e^2 / \epsilon_0 \omega^2 m^{*2}) \sum_{n,m} (2/2\pi) \int dk_z |\langle n|p|m \rangle|^2 \times [f(E_n) - f(E_m)] \times \delta(E_n - E_m - \hbar\omega). \quad (5)$$

Many commonly used approximations are not valid for calculations on bismuth nanowires. For example, since the band gap of the bismuth nanowires is less than $3k_B T$ at room temperature, the complete Fermi-Dirac distribution must be used. In addition, since the L -point bands are strongly coupled, a simple parabolic band model is insufficient, and the Lax two-band model for nonparabolic coupled bands must be used to describe the dispersion relations.²⁷ Furthermore, since the L -point electronic bands are extremely anisotropic and have strong nonparabolic effects, the calculation of the wave functions of the quantum states (as well as the coupling between these states and the joint density of states) requires a numerical calculation.

Some assumptions were made in the model presented here that in future studies should be further explored. For example, interband to intersubband coupling is not considered. Also, electron-electron interaction, including the depolariza-

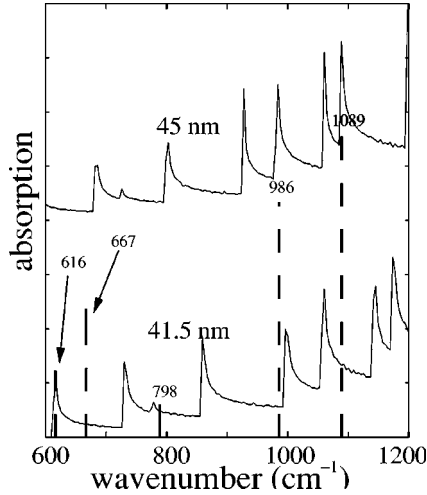


FIG. 6. The calculated optical absorption at 293 K resulting from a direct interband transition for 41.5- and 45-nm Bi nanowires oriented along the $\langle 012 \rangle$ crystalline direction. The energies and relative intensities of the experimental absorption peaks are shown by the dashed lines.

tion effect is not considered in this study. Since the electron pockets are localized in k space, the k dependence of the momentum matrix elements is not considered. Finally, only the dominant crystalline direction (012) is considered for the orientation of the Bi nanowires.

For interband transitions, transitions between the n th valence subband to the n th conduction subband are allowed. The coupling $|\langle v|p|c \rangle|$ between the valence subband v and conduction subband c , band states can be approximated by the relation

$$\frac{1}{m^*} = \frac{1}{m} + \frac{2}{m^2} \frac{|\langle v|p|c \rangle|^2}{E_g}, \quad (6)$$

where m is the free-electron mass. In the Lax two-band model, the effective mass varies with the band gap by the relation

$$\frac{1}{m^*} = \frac{1}{m} + \frac{2}{m^2} \frac{|\langle v|p|c \rangle|^2}{E_g} - \frac{12\hbar^2 k^2 |\langle v|p|c \rangle|^4}{E_g^3 m^2}. \quad (7)$$

At the band edge ($k=0$), the momentum matrix element for the different subband states is the same. In other words, as the band gap increases, the mass increases, and $|\langle v|p|c \rangle|$ remains constant.

The simulation results of the first ten interband transitions are shown in Fig. 6 for both 45- and 41.5-nm-diameter wires. Included in Fig. 6 are dashed lines (arrows) indicating the frequencies for the absorption peaks that are experimentally observed, as shown in Fig. 4. The absorption peak values observed in the ~ 45 -nm-diameter free-standing wires are included in the figure for comparison. The *calculated* absorption peak energies of interband absorption in bismuth nanowires do not agree well with the energies of the *experimentally* measured absorption peaks in the ~ 45 -nm-diameter free-standing wires in two ways. While the diameter of the

simulated wires is varied for the range of experimentally possible wire diameters, the *calculated* absorption spectra remains significantly different from that of the *measured* absorption spectra. In addition, since the conduction and valence bands do not track each other, the joint density of states for these transitions may be expected to be smaller than for the intersubband transitions, where the subbands do track each other approximately. For both these reasons, we do not believe that the measured absorption spectra are from interband transitions. Intersubband transitions are therefore considered.

The selection criteria for intersubband transitions in most systems can be summed up by a few selection rules. However, since bismuth has a very anisotropic band structure and because of the bismuth nanowire's radial symmetry, the selection rules are more complicated than for quantum wells, quantum dots, square nanowires, or even circular wires made from a material with an isotropic band structure. Therefore, a numerical method is used to solve for the oscillator strengths of the inter-subband transitions. Even though the coupling between lower-order states is strong, the lower-energy limit of our measurement setup prevents us from observing these transitions. The energy between the first and second subband edges is only 140 cm^{-1} , while the lowest energy measured by our experimental setup is 600 cm^{-1} . Therefore, only higher-order transitions with significant coupling are experimentally observed, and for this reason the model calculations include absorption from higher order states.

A more complete version of a previously published model of the electronic structure³ is used to find the energy levels and wave functions for the first 50 subbands, using a certain wire crystallographic orientation along the wire axis, and using, as variables, the wire diameter and the temperature. In this model, the change in the nonparabolicity with wire diameter is taken into account. Using the energy levels and wave functions calculated with this model, the oscillator strengths between each of the 50 states to every other 50 states are calculated. The oscillator strengths F_{nm} are found in terms of the integral

$$\begin{aligned} F_{nm} &= [2/(m^* \hbar \omega_{n,m})] |\langle n|p_{x,y}|m \rangle|^2 \\ &\propto |\langle n|p_{x,y}|m \rangle|^2 / \omega_{n,m} \\ &\propto \left| \int \psi_n (E_x \partial / \partial x + E_y \partial / \partial y) \psi_m dA \right|^2 / \omega_{n,m}, \quad (8) \end{aligned}$$

where ψ_n and ψ_m are the wave functions for the n th and m th states, and E_x and E_y are the electric-field components of the incident light perpendicular to z , the wire axis, and $\hbar \omega_{n,m}$ is the energy between states n and m . We assume that the incident light is a TEM (transverse electromagnetic wave) and hence, the integration is carried out over the cross sectional area A of the wire.

Figure 7 shows the oscillator strengths for transitions from the first ($n=0$) state to the 50 lowest states ($m=0-49$). In doing the calculations, the polarization of the incident light is varied by 5.6° increments to cover the whole 360° range. Since unpolarized light is used in our experiments, the polarization that gives the largest oscillator strength for each transition is shown in Fig. 7. The coupling

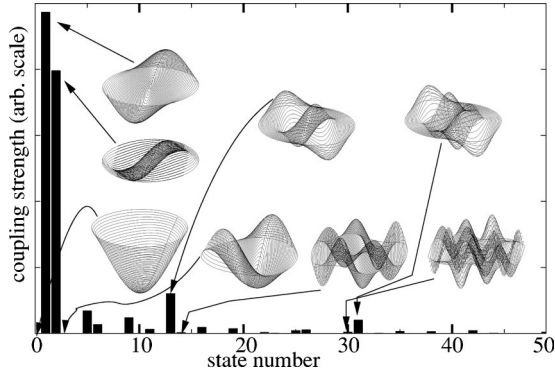


FIG. 7. The coupling term from the $n=0$ state to the $m=0$ to 49 states for carrier pocket A (see the inset of Fig. 8). The wave functions of some states are shown ($n=0, 1, 2, 3, 13, 14, 30,$ and 32). States that are radially antisymmetric have a larger coupling to the symmetric lowest-energy $m=0$ state. Also, the figure shows that even higher-order states can have a significant coupling to the $m=0$ state.

between the first 50 states, or 2500 transitions, is calculated for the three L -point carrier pockets.

Higher-order states have more nodes in their wave functions, and hence the overlap integral with the first state in general decreases with increasing n . However, this decrease is not at all monotonic, since some transitions do not allow for first-order coupling because of selection rules. Since bismuth is anisotropic, and since the circular wire only has one index number, the higher order states sometimes have only a few nodes and hence have a relatively large coupling to lower order states. The $n=32$ state is an example of a high- n state that is slowly varying with few nodes and therefore has significant coupling to the $n=0$ state. The two-dimensional wave functions of the $n=0, 1, 2, 3, 14, 15, 31,$ and 32 states in a circular bismuth nanowire are shown in Fig. 7.

The frequency dependence of $\epsilon_2(\omega)$ resulting from intersubband transitions from states $n=0-29$ to states $n=0-49$ for 41.5-nm-diameter, $\langle 012 \rangle$ oriented, bismuth nanowires at 293 K is calculated by the equation

$$\epsilon_2 \propto (1/\omega) \sum_p \sum_{n=0}^{29} \sum_{m=0}^{49} \int \delta[E_n(k) + E_m(k) - \hbar\omega] \times F_{nm} [f(E_n(k)) - f(E_m(k))] dk_z, \quad (9)$$

where the sum over p is over the three electron carrier pockets, as shown in the inset of Fig. 8, and the sums over n and m are for the initial and final states n and m . The integral includes a delta function where the energy of the incident light is equal to the energy difference between the initial and final states (n and m). The integral also includes the oscillator strength F_{nm} , as discussed above. The integral is carried out over momentum k_z in the direction of the wire axis. For all calculations in this work, the wires are assumed to be undoped, so the Fermi energy is set so that the nanowires are charge neutral. Since bismuth has both L -point and T -point valence bands, and only an L -point conduction band near the Fermi energy, the Fermi energy in undoped samples is much

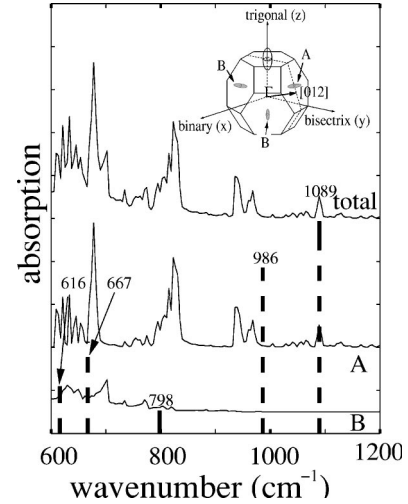


FIG. 8. The calculated optical absorption at 293 K resulting from intersubband transitions for 41.5-nm Bi nanowires oriented along the $\langle 012 \rangle$ crystalline direction. The separate contributions from the two types of electron carrier pockets A and B, as well as the total optical absorption, are presented. The energies and relative intensities of the experimental absorption peaks are shown by the dashed lines. In the inset, the Brillouin zone of bismuth is shown and the $\langle 012 \rangle$ crystalline direction is indicated by the arrow from the Γ point.

closer to the L -point conduction band than to the L -point valence band. For example, in 41.5-nm-diameter wires at room temperature, the Fermi energy lies 48 meV above the lowest L -point conduction band minimum (between the fourth and the fifth subbands) and since the band gap for the first interband transition is 97 meV (782 cm^{-1}), the Fermi energy is 145 meV above the top L -point valence subband. Because of this location of the Fermi energy, the intersubband absorption from the conduction band will dominate over the intersubband absorption from the valence band.

The resulting frequency-dependent absorption curve is shown in Fig. 8. In $\langle 012 \rangle$ -aligned Bi wires (such as our wires), two of the three electron pockets are degenerate. The two degenerate pockets are labeled “pocket B” in Fig. 8 and the third electron pocket is labeled “pocket A.” On the one hand, the optical absorption should be dominated by pocket A, since this pocket has the largest effective mass in the unconfined direction and therefore has the largest joint density of states. On the other hand, pocket B is doubly degenerate. Therefore, both types of pockets contribute significantly to the intersubband absorption spectra. Pocket A has the smaller effective mass in the confined directions, and therefore has a larger energy separation between subbands. Pocket A, hence, has larger absorption peaks separated by larger energy intervals compared to those of pocket B.

For perfectly parabolic and symmetric bands, the energy for an electron to make an $n \rightarrow m$ transition over a fixed number of states is independent of the initial state. For example, the energy for a transition between the first and third states is the same as the energy for a transition from the third to the fifth states. Even though Bi nanowires are very aniso-

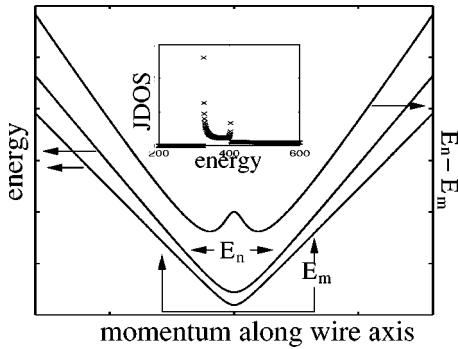


FIG. 9. Two subbands (arbitrarily labeled E_n and E_m) and the energy difference between them ($E_m - E_n$) shown as a function of momentum along the wire axis. The corresponding joint density of states (JDOS) is shown in the inset. The nonparabolic effects cause the minimum-energy difference between two subbands to be away from the subband edges. Thus the joint density of states, as shown in the inset, has two singularities: a higher-energy singularity resulting from transitions at the subband edge, and a lower-energy singularity resulting from transitions at the location of the minimum energy difference between the subbands.

tropic and non-parabolic, we see from Fig. 8 that the 1500 transitions modeled for each pocket tend to have energies similar to other transitions in that pocket, so that the complete absorption spectra includes only a few absorption peaks, each broader than the spectra resulting from a single transition. For example, the peak at around 800 cm^{-1} is a sum of the absorptions from transitions from states 3, 5, 8, and 10 to states 21, 26, 32, and 37, respectively. Similarly the absorption peak around 1100 cm^{-1} is a sum of the absorptions from transitions between states 5 and 7 with states 36 and 42, respectively. This effect is more obvious for pocket *A* than for pocket *B*, since pocket *A* has a larger energy difference between states. In addition to the transitions having similar energies, many transitions are not allowed by symmetry, or are only weakly allowed. These two effects combine to result in only 6–10 expected large absorption peaks in the frequency range between 600 and 2000 cm^{-1} .

Another interesting effect is that the nonparabolic bands cause the minimum-energy difference between two subbands to be slightly away from the band edges, as shown in Fig. 9. Therefore, for one intersubband transition, there can be two energies with singularities in the joint density of states, one at the subband separation at the band edge, and the other at the minimum energy separation between the subbands away from the band edge (see Fig. 9). The two singularities in the joint density of states cause two peaks to occur in the absorption spectra for each intersubband transition. The two asymmetric peaks have their tails facing each other, and therefore one has a positive dispersion and the other has a negative dispersion. Depending on the position of the Fermi level relative to the subband edges, either the low-energy peak, the high-energy peak, or both absorption peaks will be observed. The simulated absorption spectrum of an isolated transition as shown in the inset of Fig. 9 exhibits this double absorption peak effect, but when the absorption from all transitions are considered as in Fig. 8, this effect is washed out. The double absorption peak resulting from the nonparabolic bands in

bismuth may not be observed in wires with significant electron population, since the many-body depolarization effect can modify the line shape resulting from nonparabolic bands.²⁸

Included in Fig. 8 are dashed lines (arrows) indicating the frequencies for the absorption peaks that are experimentally observed, as shown in Fig. 4. The absorption peak values observed in the $\sim 45\text{-nm}$ -diameter free-standing wires are included on the figure for comparison. The *calculated* absorption peak energies of the 41.5-nm -diameter wires agree well with the energies of the *experimentally* measured absorption peaks in the $\sim 45\text{-nm}$ -diameter free-standing wires. The agreement between the experimental and model results is quite good, considering that the room-temperature bismuth band parameter data used for the calculations are not accurately determined,²⁹ that the wire diameters are only known to $\pm 5\text{ nm}$ (as discussed above in connection with the oxide coating), and that the Fermi energy is not independently known. However, the ratio of the absorption peak intensities do not agree well with theory. From Fig. 4 we see that the experimental 1089-cm^{-1} absorption peak is significantly larger than the peaks at ~ 616 , ~ 667 , and $\sim 798\text{ cm}^{-1}$. In the simulations, the 1089-cm^{-1} peak is relatively small, since the absorption peak intensities decrease with increasing wave number, because of the decreasing coupling, as shown in Fig. 7. The difference in the peak intensities between theory and experimental results could well be explained by other absorption mechanisms contributing to the absorption at around 1100 cm^{-1} . One such possible absorption mechanism is the indirect transition between the holes in the *T*-point valence band and the *L*-point valence band. For semi metallic bismuth nanowires, the hole concentration at the *T*-point is large enough and the *T*- and *L*-point valence bands track each other well enough so that this indirect transition could give significant absorption at room temperature. In addition, preliminary simulations of the absorption spectra for a 40-nm wire show that indirect interband absorption has an energy threshold around 1100 cm^{-1} with continued absorption for higher energies, and the preliminary simulation results also show a very narrow absorption peak for the indirect absorption process around 1200 cm^{-1} . Furthermore, the sharp absorption peak from the indirect *L-T* point transition shifts to higher energies with decreasing wire diameter at a rate about equal to the observed shift of the 1000-cm^{-1} peak with wire diameter. The simulated absorption peaks, resulting from intersubband transitions increase in energy at a faster rate with decreasing wire diameter than the rate experimentally observed for the 1000-cm^{-1} peak.¹¹

It is also possible that effects not included in the our present model, such as the surface roughness of the wire, wire to wire coupling, many-electron effects, and limits to the infinite barrier approximation, could give rise to the differences between the measured and predicted absorption spectra. Temperature dependent absorption measurements and further simulation of the indirect transition, both of which we are now pursuing in depth, are needed to establish the absorption mechanism definitively.

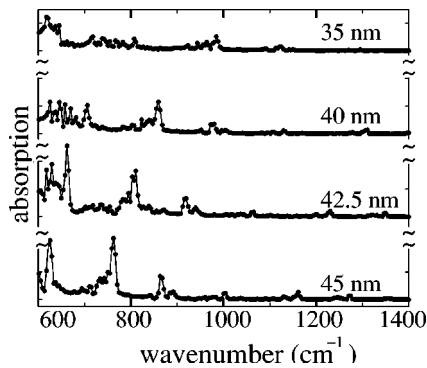


FIG. 10. Simulated energy dependence of the intersubband absorption at 293 K for 45-, 42.5-, 40-, and 35-nm-diameter wires. As the wire diameter decreases, the number of absorption peaks increases and the absorption peak intensities decrease.

The modeled intersubband absorption results for $\langle 012 \rangle$ bismuth nanowires with diameters of 35, 40, 42.5, and 45 nm at 293 K, are shown in Fig. 10. As the wire diameter is decreased, more absorption peaks appear with decreasing intensity. From this figure, we also observe an increase in the energy of the peak positions as the wire diameter is decreased. The sensitivity of the absorption peaks to the wire diameter should enable optical measurements to accurately determine the wire diameters when the band parameters are well known.

V. CONCLUSIONS

In this paper, intersubband and interband absorptions of bismuth nanowires are modeled and compared to experimental results. Five absorption peaks were observed experimen-

tally, and the energies of these five peaks agree well with the simulated intersubband absorption curve for 41.5-nm wires. We therefore conclude that the absorption peaks are from intersubband transitions resulting from quantum confinement in the bismuth nanowires, and that our model for the quantum confinement of conduction electrons and valence-band holes in bismuth nanowires is valid. We compare the absorption spectra of bismuth nanowires inside an alumina template obtained by a reverse EMT to that of free-standing bismuth nanowires with a bismuth oxide coating. The good agreement in the absorption peak energy at $\sim 1050 \text{ cm}^{-1}$ between these two methods validates the use of the reverse EMT approach for measuring large absorption peaks at wavelengths larger than the feature size of the sample. The broader peak width in the free-standing wires is attributed to a larger effective wire diameter distribution resulting from oxide formation.

ACKNOWLEDGMENTS

The authors greatly appreciate the useful discussions with Professor P. Hagelstein, Professor Q. Hu, Dr. Gene Dresselhaus, and Professor P. Wolff. We also thank Megha Padi, Dr. Antonio Gomes de Souza Filho, Dr. Melissa Sander, Dr. Anu Agarawal, and Tim McClure for their help with this research. In addition we acknowledge Professor Narayanamurti and Stephan Shepard for their help in obtaining a thin film of bismuth used for the background spectra. The authors also acknowledge NSF Grant No. DMR-01-16042, U.S. Navy Contract No. N00167-98-K0024, and MURI Subcontract No. 0205-G-BB8531 for support. This work made use of MRSEC Shared Facilities supported by the National Science Foundation Contract No. DMR-9400334.

*Electronic mail: mrb@mit.edu

¹R.T. Isaacson and G.A. Williams, *Phys. Rev.* **185**, 682 (1969).

²Y.-M. Lin, S.B. Cronin, J.Y. Ying, M.S. Dresselhaus, and J.P. Heremans, *Appl. Phys. Lett.* **76**, 3944 (2000).

³Y.M. Lin, X. Sun, and M.S. Dresselhaus, *Phys. Rev. B* **62**, 4610 (2000).

⁴G. Dresselhaus, M.S. Dresselhaus, Z. Zhang, X. Sun, J. Ying, and G. Chen, in *Seventeenth International Conference on Thermoelectrics: Proceedings, ICT'98; Nagoya, Japan*, edited by K. Koumoto (Institute of Electrical and Electronics Engineers, Piscataway, NJ, 1998), pp. 43-46.

⁵Z. Zhang, J. Ying, and M. Dresselhaus, *J. Mater. Res.* **13**, 1745 (1998).

⁶J. Heremans, C.M. Thrush, Y. Lin, S. Cronin, Z. Zhang, M.S. Dresselhaus, and J.F. Mansfield, *Phys. Rev. B* **61**, 2921 (2000).

⁷G.L. Hornyak, C.J. Patrissi, and C.R. Martin, *J. Phys. Chem. B* **101**, 1548 (1997).

⁸C.A. Foss, Jr., G.L. Hornyak, J.A. Stockert, and C.R. Martin, *J. Phys. Chem. B* **98**, 2963 (1994).

⁹D.E. Aspnes, *Thin Solid Films* **89**, 249 (1982).

¹⁰N.L. Cherkas, *Opt. Spectrosc.* **81**, 990 (1996) [*Opt. Spectrosc.* **81**, 906 (1996)].

¹¹M.R. Black, M. Padi, S.B. Cronin, Y.-M. Lin, O. Rabin, T. Mc-

Clure, G. Dresselhaus, P.L. Hagelstein, and M.S. Dresselhaus, *Appl. Phys. Lett.* **77**, 4142 (2000).

¹²D.E. Aspnes, A. Heller, and J.D. Porter, *J. Appl. Phys.* **60**, 3028 (1986).

¹³J.C. Maxwell Garnett, *Philos. Trans. R. Soc. London, Ser. A* **203**, 385 (1904).

¹⁴J.C. Maxwell Garnett, *Philos. Trans. R. Soc. London, Ser. A* **205**, 237 (1906).

¹⁵C.A. Foss, G.L. Hornyak, Jr., J.A. Stockert, and C.R. Martin, *J. Phys. Chem.* **96**, 7497 (1992).

¹⁶A. Anderson, O. Hunderi, and C.G. Granqvist, *J. Appl. Phys.* **51**, 754 (1980).

¹⁷V.V. Poborchii, *Jpn. J. Appl. Phys.* **34**, 271 (1995).

¹⁸P.N. Sen, C. Scala, and M.H. Cohen, *Geophysics* **46**, 781 (1981).

¹⁹U. Kreibig, A. Althoff, and H. Pressmann, *Surf. Sci.* **106**, 308 (1991).

²⁰U. Kreibig and L. Genzel, *Surf. Sci.* **156**, 678 (1985).

²¹S. Link, M.B. Mohamed, and M.A. El-Sayed, *J. Phys. Chem. B* **103**, 3073 (1999).

²²C.G. Granqvist and O. Hunderi, *Phys. Rev. B* **18**, 2897 (1978).

²³J.W. Diggle, T.C. Downie, and C.W. Goulding, *Chem. Rev.* **69**, 365 (1969).

²⁴J.P. Sullivan and G.C. Wood, *Proc. R. Soc. London, Ser. A* **317**, 511 (1970).

- ²⁵S.B. Cronin, Y.-M. Lin, P.L. Gai, O. Rabin, M.R. Black, G. Dresselhaus, and M.S. Dresselhaus, in *Anisotropic Nanoparticles: Synthesis, Characterization and Applications: MRS Symposium Proceedings, Boston, December 2000*, edited by S. Stranick, P.C. Searson, L.A. Lyon, and C. Keating, (Materials Research Society, Pittsburgh, 2001), pp. c571–c576.
- ²⁶The present paper extends to 1D the derivation of Eq. (3) given for 2D by H. C. Lui, in *Semiconductors and Semimetals*, Vol. 62 (Academic, San Diego, CA, 2000).
- ²⁷B. Lax, J.G. Mavroides, H.J. Zeiger, and R.J. Keyes, *Phys. Rev. Lett.* **5**, 241 (1960).
- ²⁸M. Zaluzny, *Phys. Rev. B* **43**, 4511 (1991).
- ²⁹M.P. Vecchi and M.S. Dresselhaus, *Phys. Rev. B* **10**, 771 (1974).